MATHEMATICAL MODELING AND COMPUTING, Vol. 8, No. 1, pp. 43–57 (2021)

Calculation of stable and unstable periodic orbits in a chopper-fed DC drive

Kuznyetsov O. O.

Hetman Petro Sahaidachnyi National Army Academy,
32 Heroiv Maidanu Str., 79026, Lviv, Ukraine

(Received 29 October 2020; Revised 30 November 2020; Accepted 1 December 2020)

It is well known that electric drives demonstrate various nonlinear phenomena. In particular, a chopper-fed analog DC drive system is characterized by the route to chaotic behavior though period-doubling cascade. Besides, the considered system demonstrates coexistence of several stable periodic modes within the stability boundaries of the main period-1 orbit. We discover the evolution of several periodic orbits utilizing the semi-analytical method based on the Filippov theory for the stability analysis of periodic orbits. We analyze, in particular, stable and unstable period-1, 2, 3 and 4 orbits, as well as independent on stability they are significant for the organization of phase space. We demonstrate, in particular, that the unstable periodic orbits undergo border collision bifurcations; those occur according to several scenarios related to the interaction of different orbits of the same period, including persistence border collision, when a periodic orbit is changed by a different orbit of the same period, and birth or disappearance of a couple of orbits of the same period characterized by different topology.

Keywords: *DC drive, stability, periodic orbits, bifurcations.*
2010 MSC: 37C75, 37G15, 37N35, 37M20 **DOI:** 10.23939/mmc2021.01.043

1. Introduction

It is known that electric drives being fed from power electronic converters may demonstrate nonlinear phenomena related to switching in the converter [1]. For example, it was demonstrated by Chau et al. in [2], that a simple chopper-fed DC drive (Fig. 1) with the change of input voltage or feedback gain leaves its stability region of period-1 operation associated with the period-doubling cascade.

Later on, Okafor et al. [3] reported the coexistence of multiple attractors (several stable orbits exist simultaneously for the same set of parameters) in a DC-drive with a full-bridge converter. It was also demonstrated that coexisting behavior remained unobserved in the previous numerical experiments due to the smooth change of initial conditions in the previous numerical simulations. In [4], the same behavior was reported for the topology as in Fig. 1. In particular, it was demonstrated that for feedback gain $g = 2$, the stable period-1, 3 and 4 modes coexist. The boundaries of stability for those modes as g changes were discovered utilizing Filippov theory.

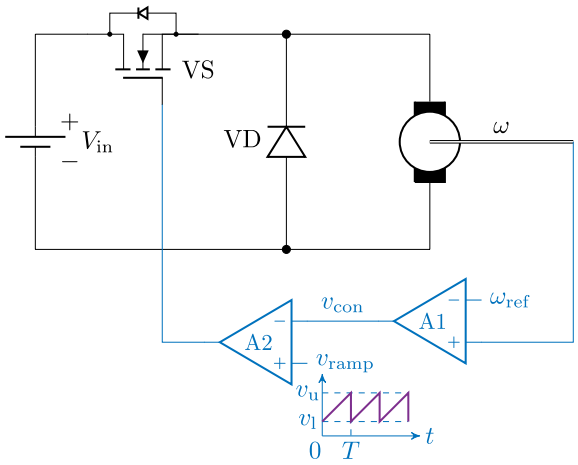

Fig. 1. Circuit diagram of an analog chopper-fed DC drive [2].

It should be noted that in [4], stable orbits were analyzed. However, unstable orbits play an important role in the organization of state space as well [5]. They cannot be detected neither experimentally nor from numerical simulations, but may cause different nonlinear effects in a system. As a consequence, [6] proposes to analyze nonlinear systems by finding periodic solutions up to period nT ($n = 1, 2, 3, \ldots$,

where T is the period of the main period-1 solution), both stable and unstable, with the next continuation along those solutions. These ideas were successfully implemented in [7] for the problems of detecting of so-called "rare attractors" — those are stable periodic orbits existing in a narrow range of the varying parameter. The same "rare attractors" were observed in a switching power converter [8, 9]. Reference [9] examined the effect of switching delays on the previously reported behavior.

In the present study, we follow [4] by applying the Filippov theory for the analysis of periodic orbits in a DC drive system. The theory itself is exposed in [10], and it was implemented in [11] for the stability analysis of periodic orbits in switching power converters. In the literature, [11] is often referred to as the first application of the theory to power electronic area; however, for our knowledge, the first application of the theory to stability analysis of power electronic circuits belongs to [12]. Following [11], Mandal et al. [13, 14] proposed an algorithm for the detection of (un)stable periodic orbits in hybrid dynamical systems depicted by ordinary differential equation (ODE) systems. Due to their nature, associated with different topology for different state of power switches, power electronic and drive systems are suitable case studies for the algorithm. Recently, the Filippov theory was extended to the analysis of switching power converters modeled as hybrid differential algebraic equations (DAE) systems as well [15].

It should be noted that Filippov theory can be applied not only for the analysis, as in [16], but also to control the stability of a periodic orbit [17, 18].

In the current study, we apply the ideas in [6, 7] for the analysis of (un)stable periodic orbits in the simple chopper-fed DC drive (Fig. 1). This extends the results obtained in [4], where only stable periodic orbits were analyzed. For those purposes, we apply Filippov theory and the modified algorithm from [13].

2. Description of the system

We consider a chopper-fed permanent magnet DC drive with the speed feedback loop and an analog control circuit (Fig. 1 [2]) operating in a continuous conduction mode. ODE system describing the considered simple DC drive depends on the state of the switch VS (Fig. 1). Thus, when $v_{\text{con}} < v_{\text{ramp}}$ the switch is on

$$\frac{\mathrm{d}}{\mathrm{d}t}\begin{bmatrix} \omega(t) \\ i(t) \end{bmatrix} = \begin{bmatrix} -\frac{B}{J} & \frac{K_T}{J} \\ -\frac{K_E}{L} & -\frac{R}{L} \end{bmatrix}\begin{bmatrix} \omega(t) \\ i(t) \end{bmatrix} + \begin{bmatrix} -\frac{T_{\text{L}}}{J} \\ \frac{V_{\text{in}}}{L} \end{bmatrix}, \tag{1}$$

and when $v_{\text{con}} \geqslant v_{\text{ramp}}$ the switch is off

$$\frac{\mathrm{d}}{\mathrm{d}t}\begin{bmatrix} \omega(t) \\ i(t) \end{bmatrix} = \begin{bmatrix} -\frac{B}{J} & \frac{K_T}{J} \\ -\frac{K_E}{L} & -\frac{R}{L} \end{bmatrix}\begin{bmatrix} \omega(t) \\ i(t) \end{bmatrix} + \begin{bmatrix} -\frac{T_{\text{L}}}{J} \\ 0 \end{bmatrix}. \tag{2}$$

Both (1) and (2) in state-space are represented as

$$\dot{\mathbf{x}} = \mathbf{A}\,\mathbf{x} + \mathbf{E}_k, \quad (k = \text{on},\ \text{off}) \tag{3}$$

where

$$\mathbf{A} = \begin{bmatrix} -B/J & K_T/J \\ -K_E/L & -R/L \end{bmatrix}, \quad \mathbf{x} = \begin{bmatrix} \omega(t) \\ i(t) \end{bmatrix}, \quad \mathbf{E}_{\text{off}} = \begin{bmatrix} -T_{\text{L}}/J \\ 0 \end{bmatrix}, \quad \mathbf{E}_{\text{on}} = \begin{bmatrix} -T_{\text{L}}/J \\ V_{\text{in}}/L \end{bmatrix}.$$

Matrix $\mathbf{E}_k$ is equal to the product $\mathbf{B}\,\mathbf{u}$ form the standard state-space representation.

The power switch VS changes its state to the other one each time when both voltages (4) and (5) are equal, or when after the time event associated with the ramp signal v_{ramp}, the relation between v_{con} and v_{ramp} changes.

In Fig. 1, the carrier signal voltage (ramp voltage) is a sawtooth wave characterized on the ramp period T as

$$v_{\text{ramp}}(t) = v_{\text{l}} + (v_{\text{u}} - v_{\text{l}}) \left(\frac{t}{T} \mod 1 \right), \tag{4}$$

ramping upward from the lower v_{l} to the upper v_{u} level voltage. In the considered case study, a proportional speed controller is utilized, therefore, the control signal v_{con} is proportional to the difference between the instantaneous speed $\omega(t)$ and the reference speed ω_{ref}:

$$v_{\text{con}}(t) = g\,(\omega(t) - \omega_{\text{ref}})\,, \tag{5}$$

where g is a feedback gain.

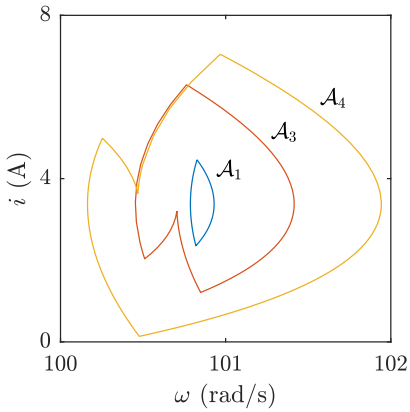

Fig. 2. Phase portraits of the co-existing period-1, 3 and 4 attractors $\mathcal{A}_i$, $i = \{1, 3, 4\}$ for $g = 2$.

The equations in the subsection are based on [2], and the parameters of the drive system are taken from [2] as well (provided in Appendix). Note, that we follow [2] by considering the operation with low switching frequency (250 Hz) in order to simplify the model by neglecting parasitic reactance and amplification of switching noise, thus focusing on the main theoretical results [1].

As it was mentioned earlier in the Introduction, [4] reported the coexistence of three stable attracting sets for the same parameters as we use in our study. Applying the mathematical description of the system (1)–(5) in Matlab environment, we have evaluated those attractors (Fig. 2) as well as trajectories referred to period-1, 3 and 4 modes (Fig. 3).

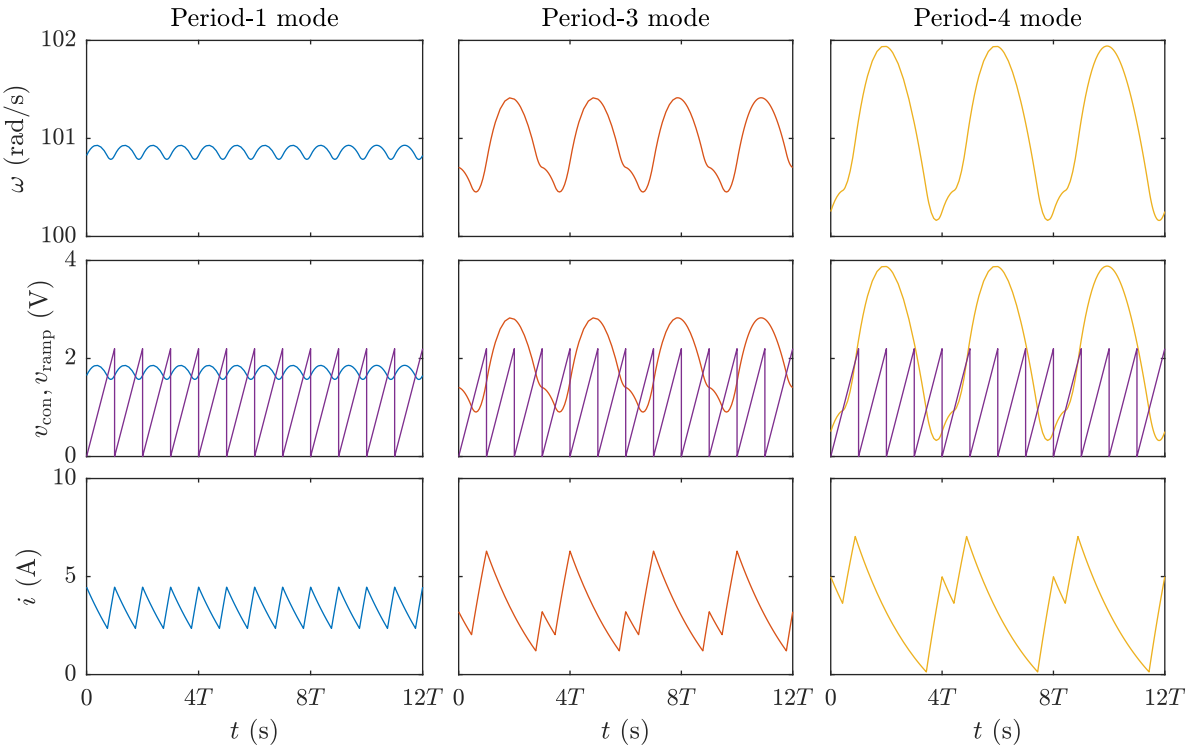

Fig. 3. Trajectories of the co-existing period-1, 3 and 4 modes for $g = 2$.

3. Filippov theory and its application for the analysis of electric drive systems

3.1. Outline of the Filippov theory

For the switching power converters, their dynamics is governed by the clock, characterized by period T, responsible for the generation of the ramp signal v_{ramp}. Therefore, an n-periodic orbit depicts a transition in the state space from a state $\mathbf{x}_0 = \mathbf{x}(0)$ at a clock instant to the same state after n clock periods: $\mathbf{x}_0 = \mathbf{x}(nT)$. An electric drive system with a power electronic converter in the state space is split into at least two partitions with periodically moving borders [19]. We consider each partition as a linear time-invariant (LTI) system depicted by an equation $\dot{\mathbf{x}} = \mathbf{A}\,\mathbf{x} + \mathbf{B}\,\mathbf{u}$.

Below, we present the Filippov theory from the point of view of the analysis of the switching converters [11].

In each subsystem, their transition from $\mathbf{x}(t_0)$ to $\mathbf{x}(t)$ is governed by the state transition matrix $\mathbf{\Phi}(t, t_0) = e^{\mathbf{A}(t-t_0)}$ so as:

$$\mathbf{x}(t) = \mathbf{\Phi}(t, t_0)\,\mathbf{x}(t_0).$$

Thus, the evolution of perturbation:

$$\Delta\mathbf{x}(t) = \mathbf{\Phi}(t, t_0)\,\Delta\mathbf{x}(t_0).$$

When the state crosses the border between the two subsystems depicted by the vector fields $\mathbf{f}_-$ and $\mathbf{f}_+$, the state transition matrix (saltation matrix) describes a relation of the perturbation just after the event $\Delta\mathbf{x}(t_+)$ to that just before $\Delta\mathbf{x}\,(t_-)$:

$$\Delta\mathbf{x}(t_+) = \mathbf{S}\,\Delta\mathbf{x}(t_-).$$

In Filppov theory, the saltation matrix for a switching event at t_{sw} is derived in the form [11]:

$$\mathbf{S} = \mathbf{I}_N + \frac{(\mathbf{f}_+ - \mathbf{f}_-)\,\mathbf{n}^\top}{\mathbf{n}^\top\mathbf{f}_- + \frac{\partial h}{\partial t}\big|_{t=t_{\text{sw}}}}, \tag{6}$$

where $\mathbf{I}_N$ is identity matrix of order N, where N is the number of dimensions of the state space, the hypersurface in the state space Σ is represented by the switching condition $h\,(\mathbf{x}, t) = 0$, $\mathbf{n}$ is the vector normal to Σ, $(\cdot)^\top$ is transpose operator.

For an n-periodic cycle, the evolution of the perturbation is governed by the monodromy matrix $\mathbf{M}$, so as

$$\Delta\mathbf{x}(t_0 + nT) = \mathbf{M}\,\Delta\mathbf{x}(t_0),$$

and the same can written for the evolution of the state:

$$\mathbf{x}(t_0 + nT) = \mathbf{M}\,\mathbf{x}(t_0).$$

Consequently, $\mathbf{M}$ is utilized as the Jacobian matrix around the periodic steady-state for the analysis of its stability [14]. Therefore, the eigenvalues of the monodromy matrix $\lambda_i\,(i = 1, \ldots, N)$ are utilized to study the stability of a periodic orbit according to the relation $|\lambda_i| < 1$ (all eigenvalues should lie inside a unit circle).

3.2. Calculation of stability of periodic orbits utilizing Filippov theory

Let the dynamical system moving around the periodic orbit m times crosses the switching hypersurfaces. For the generalization, let there be m different subspaces, therefore, the same number of the switching hypersurfaces $\Sigma_i\,(i = 1, \ldots, m)$ and transition between the subsystems are governed by the

saltation matrices $\mathbf{S}_i$. The transition over a cycle nT is governed by the monodromy matrix:

$$\mathbf{M} = \mathbf{S}_m \times \mathbf{\Phi}_m \times \mathbf{S}_{m-1} \times \mathbf{\Phi}_{m-1} \times \ldots \times \mathbf{S}_2 \times \mathbf{\Phi}_2 \times \mathbf{S}_1 \times \mathbf{\Phi}_1. \tag{7}$$

Detection and continuation of periodic orbits utilizing Filippov theory is based on the algorithm described in [13]. First, let us assume that we have *a priori* information about the periodic orbit: an initial state $\mathbf{x}_0$ and the sequence of subsystems visited by the orbit. Initial state of the periodic orbit can be obtained by integration the ODE system representing the model until steady-state is obtained.

Afterwards, starting from $\mathbf{x}_0$ we integrate the ODE system until the switching event is detected. In the current study, we have utilized standard Matlab function `ode45` realizing the explicit Runge-Kutta method of order 4, 5. Event detection was implemented utilizing the built-in ODE solver feature. When a switching instant t_i is detected, the matrices $\mathbf{x}_i$, $\mathbf{\Phi}_i$ and $\mathbf{S}_i$ are calculated as it was described above in the subsection 3.1. In the end, when the state $\mathbf{x}_m$ is obtained (it should be equal to $\mathbf{x}_0$), the monodromy matrix is calculated after (7). The resulting decision on the stability of the orbit is based on the eigenvalues of $\mathbf{M}$.

It should be noted that in [13], the algorithm requires no *a priori* information about the sequence of subsystems. That means, the form of the expression for each $\mathbf{S}_i$ is *a priori* unknown, it depends on the type of event detected. Those operations are simply implemented with built-in Matlab ODE solver.

However, in our study we have utilized both algorithms–"manual" and "automatic." The details for the use of both algorithms will be provided below in subsection 4.7.

3.3. Continuation of periodic orbits utilizing Filippov theory

The detection of a periodic orbit is based on an initial guess $\mathbf{x}_0'$, that can be obtained by the straightforward integration of the ODE system. Afterwards, Newton–Raphson search routine is applied with the next step $\mathbf{x}_0'$ given as [13, 14]:

$$\mathbf{x}_0' = \mathbf{x}_0 - \left(\frac{\partial \mathbf{x}_m}{\partial \mathbf{x}_0} - \mathbf{I}_N \right)^{-1} (\mathbf{x}_m - \mathbf{x}_0) \,. \tag{8}$$

Since

$$\frac{\partial \mathbf{x}_m}{\partial \mathbf{x}_0} = \frac{\partial \mathbf{x}_m}{\partial \mathbf{x}_{m-1}} \times \mathbf{S}_{m-1} \times \frac{\partial \mathbf{x}_{m-1}}{\partial \mathbf{x}_{m-2}} \times \mathbf{S}_{m-2} \times \ldots \times \frac{\partial \mathbf{x}_2}{\partial \mathbf{x}_1} \times \mathbf{S}_1 \times \frac{\partial \mathbf{x}_1}{\partial \mathbf{x}_0} = \mathbf{M}, \tag{9}$$

then partial derivative in (8) is a monodromy matrix, and (8) is converted to

$$\mathbf{x}_0' = \mathbf{x}_0 - (\mathbf{M} - \mathbf{I}_N)^{-1} (\mathbf{x}_m - \mathbf{x}_0) \,. \tag{10}$$

With the obtained new value of $\mathbf{x}_0$ as an initial guess, we repeat the described above search routine with the parameter slightly varied. Updating the state transition and saltation matrices, and as a result, new monodromy matrix, a new periodic orbit is obtained after (10). Thus, the evolution of the periodic orbit is discovered independent on its stability.

3.4. Saltation matrices of the DC drive

To calculate saltation matrices for the system under study, we require the expressions for the switching hypersurfaces Σ_i and the normals to them $\mathbf{n}_i$. The following expressions are adapted from [4], where the system is examined.

Thus, when the switching instant is associated with the equality of (4) and (5), the switching hypersurface is given by

$$\Sigma_1 = \{(\mathbf{x}, t) | h_1(\mathbf{x}, t) = 0\} \,,$$

where

$$h_1(\mathbf{x},t) = v_{\text{con}}(t) - v_{\text{ramp}}(t) = g\,(\mathbf{x}_1 - \omega_{\text{ref}}) - \left(v_{\text{l}} + (v_{\text{u}} - v_{\text{l}})\frac{t}{T}\right). \tag{11}$$

Therefore, the partial derivative from (11):

$$\frac{\partial h_1}{\partial t} = -\frac{v_{\text{u}} - v_{\text{l}}}{T}, \tag{12}$$

the normal vector is

$$\mathbf{n} = \begin{bmatrix} \frac{\partial h_1}{\partial \mathbf{x}_1} \\ \frac{\partial h_1}{\partial \mathbf{x}_2} \end{bmatrix} = \begin{bmatrix} g \\ 0 \end{bmatrix}. \tag{13}$$

Equations (11) and (12) are substituted into (6) to obtain the expression of $\mathbf{S}_1$ related to the crossing of switching hypersurface.

If the switching is associated with the time event (the end of the switching period) $t = nT$, then $\frac{\partial h_2}{\partial t} = \infty$ due to discontinuity of $v_{\text{ramp}}(t)$. Substituting infinity into denominator into (6), we obtain the saltation matrix $\mathbf{S}_2 = \mathbf{I}_N$.

4. Analysis of the periodic orbits in a DC drive

4.1. A glimpse at the structure of periodic orbits

We have constructed the bifurcation diagrams for the stroboscopic map $\mathbf{x}_{n+1} = P(\mathbf{x}_n)$, where $\mathbf{x}_i$ is the state at $t = iT$. We analyze periodic orbits of different order as the bifurcation parameter g changes, taking into account stability of the orbits (Fig. 4). Here and below, we use blue lines for stable periodic orbits, whereas yellow — for unstable ones.

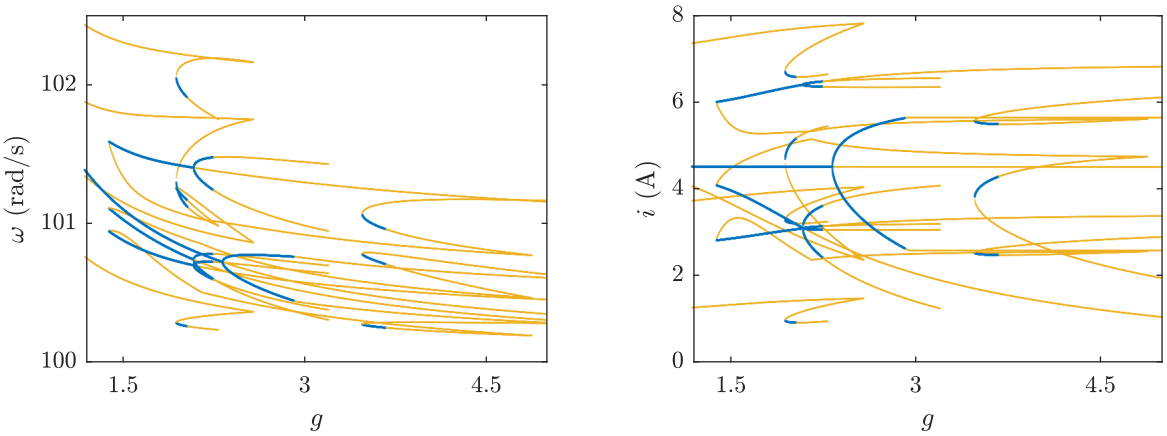

Fig. 4. General structure of the bifurcation diagram of period-1, 2, 3, 4 and 6 orbits of the DC drive: speed ω and current i with the change of feedback gain g. Here and below, we use blue lines to indicate stable periodic orbits, whereas yellow — for unstable ones.

While the stable period-1, 3 and 4 orbits that coexist in some range of gain g were analyzed in [4], the unstable ones still remain undiscovered.

Below, we use the following notation of orbits: $\mathcal{O}_{n,i}$ denotes period-n orbit, i is the sequence number, if more than one orbit of period nT exist; superscript 's' or 'u' is used to distinguish stable and unstable orbits.

4.2. Analysis of the period-1 orbit $\mathcal{O}_1$

Period-1 orbit desnotes the main operating mode the drive system is designed for (Fig. 5). As it was demonstrated by Okafor in [4], complex conjugate eigenvalues of the monodromy matrix have the same absolute value below $g = 2.302$ while their imaginary parts decrease; afterward, one of real eigenvalues moves to the border of the unit circle at -1, while the other–to the center of the circle (Fig. 6). At $g = 2.337$, the first one leaves the unit circle at the point -1. That means, $\mathcal{O}_1$ loses stability through period-doubling bifurcation causing the smooth birth of a period-2 orbit.

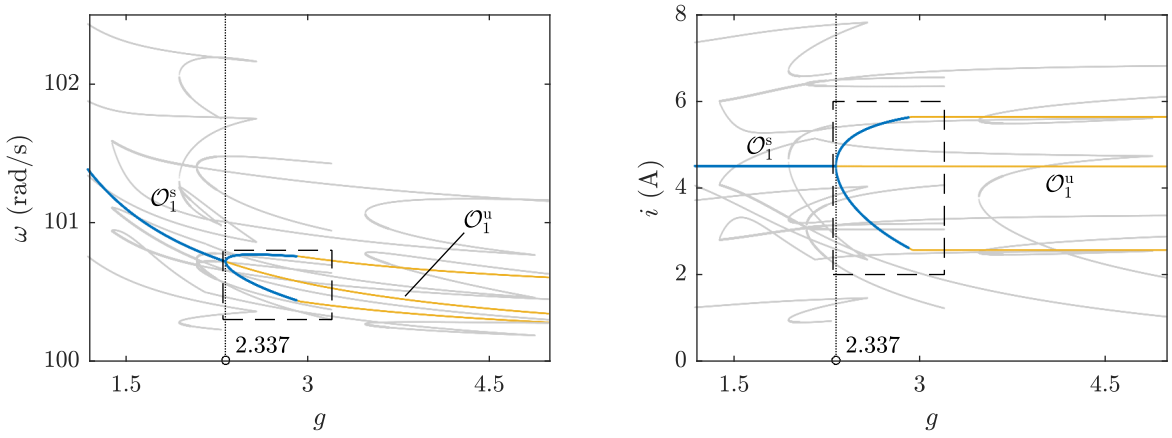

Fig. 5. Period-1 and period-2 orbits of the DC drive: speed ω and current i with the change of feedback gain g; other orbits are shaded in gray. The highlighted region is blown-up in Fig. 7.

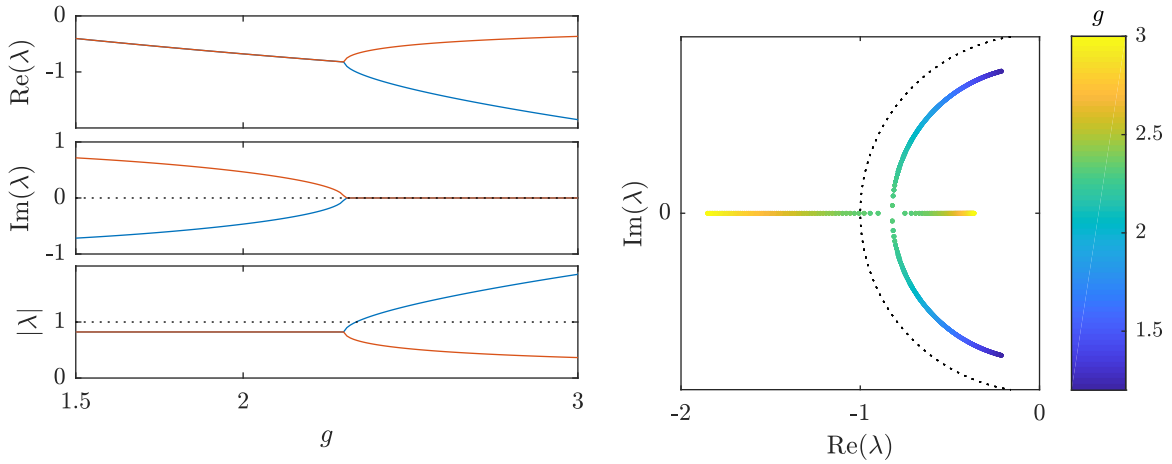

Fig. 6. Eigenvalues λ_1, λ_2 of period-1 orbit $\mathcal{O}_1$: real and imaginary parts, absolute values, and eigenvalue loci.

4.3. Analysis of the period-2 orbits $\mathcal{O}_{2,i}$

The newborn period-2 orbit $\mathcal{O}_{2,1}$ undergoes the same period-doubling scenario as in the case of $\mathcal{O}_1$; at $g = 2.923$ it becomes unstable (Fig. 7) with the birth of period-4 orbit, that is not analyzed here.

As with the increase of g the switching instant t_1 approaches the value T; at $g = 2.95$, it arrives to the end of the first period, and the structure of trajectory changes (Fig. 8, where the regions of interest are highlighted by circles). $\mathcal{O}_{2,1}$ disappears, and a new period-2 trajectory $\mathcal{O}_{2,2}$ is born through border collision bifurcation.

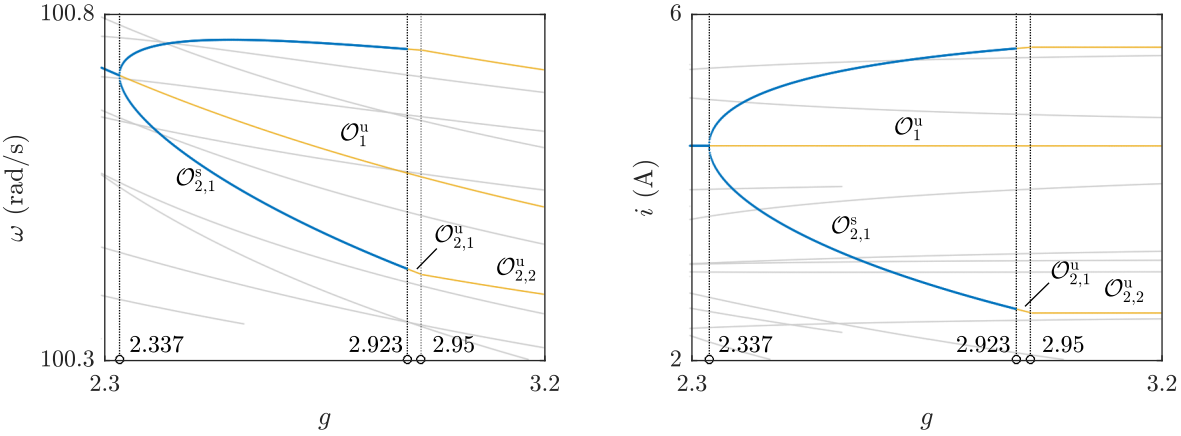

Fig. 7. Blow-up of Fig. 5 demonstrating period-2 orbits $\mathcal{O}_{2,i}$.

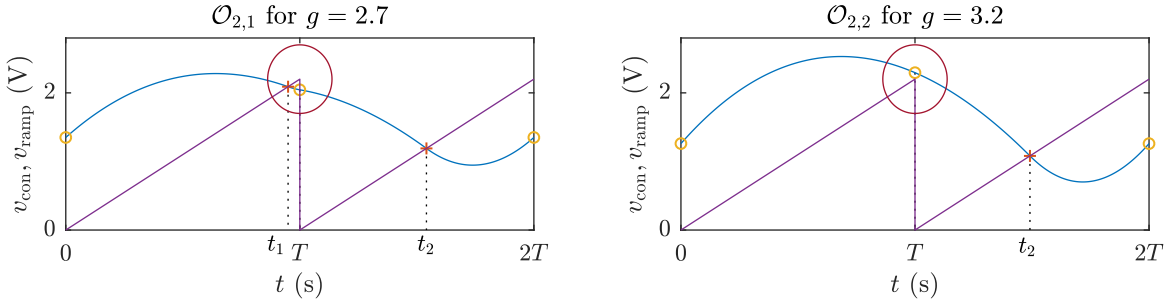

Fig. 8. Period-2 trajectories: before border collision for $g = 2.7$, after border collision for $g = 3.2$.

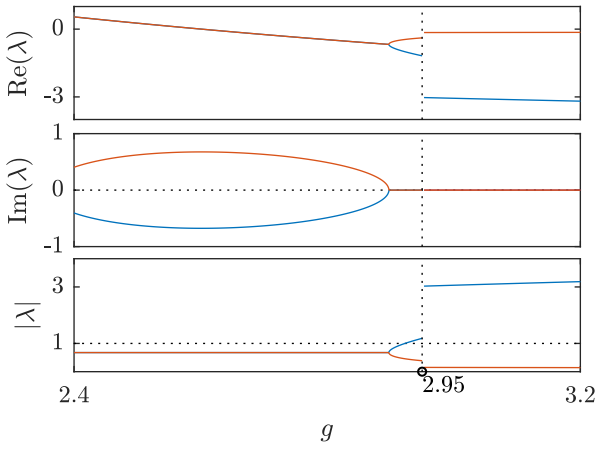

Fig. 9. Eigenvalues characterizing the period-2 orbits before and after border collision at $g = 2.95$.

Let us introduce the following symbolic representation: 1 denotes 'off' state of the switch, when $v_{\mathrm{con}} > v_{\mathrm{ramp}}$, and 2 – 'on' state when $v_{\mathrm{con}} < v_{\mathrm{ramp}}$ (the numbers may be interpreted as the sequence number of a subsystem visited by the trajectory). Therefore, we represent an orbit as a sequence of those states. For the simplicity, let separate periods be divided by dashes.

Thus, from the point of view of symbolic representation, at $g = 2.95$, we have a transition from the orbit characterized by $(12 - 12)$ to the one characterized by $(1 - 12)$. Disappearance of $\mathcal{O}_{2,1}$ and the birth of $\mathcal{O}_{2,2}$ is also observed as new eigenvalues set suddenly appearing at $g = 2.95$, while the previous set disappears (Fig. 9).

4.4. Analysis of the period-3 orbits $\mathcal{O}_{3,i}$

Unlike those analyzed before, the behavior of orbits $\mathcal{O}_{3,i}$, $i = 1, 2 \ldots 5$ is quite complicated (Fig. 10); up to four period-3 orbits may coexist for the same g value. Therefore, we analyze their behavior using the third iterate of the stroboscopic map $\mathbf{x}_{n+1} = P^3(\mathbf{x}_n)$ to separate one of the subbranches from Fig. 10 (Fig. 11). Note, that in Fig. 10, numerical values of g are labeled, while in Fig. 11, characteristic points are labeled as A to F. Below, we analyze each of the orbits and the transitions between them.

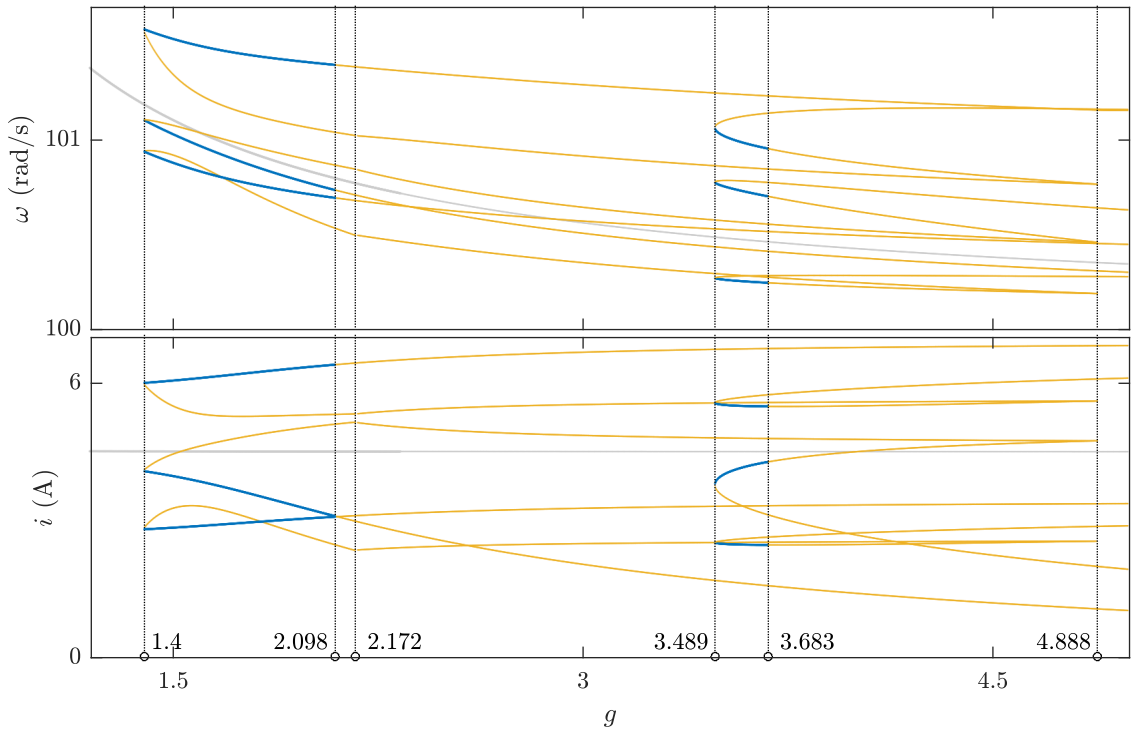

Fig. 10. Period-3 orbits of the DC drive; period-1 orbit is shaded in gray.

First, at $g = 1.4$ (at A in Fig. 11), two orbits $\mathcal{O}_{3,1}$ and $\mathcal{O}_{3,2}$ are born via the border collision bifurcation. Both of them are characterized by different symbolic sequences: $\mathcal{O}_{3,1}$ — by the sequence $(12-1-12)$, and $\mathcal{O}_{3,2}$ — by the sequence $(12-12-12)$ (Fig. 12). Point A corresponds to the case when $v_{\text{con}} = v_{\text{ramp}}$ at $t = 2T$. Hereat, $\mathcal{O}_{3,1}$ is stable, while $\mathcal{O}_{3,2}$– unstable.

The stable orbit $\mathcal{O}_{3,1}$ at $g = 2.098$ undergoes period-doubling bifurcation (B in Fig. 11) and becomes unstable. No other behavior is observed.

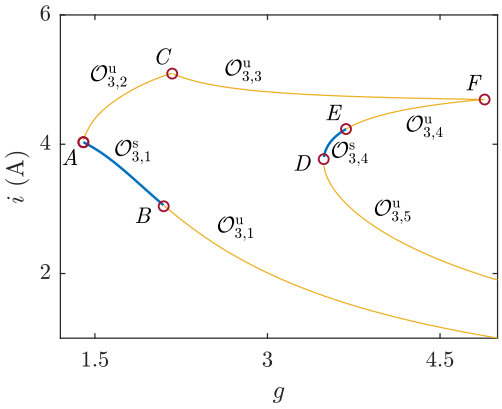

Fig. 11. Schematic of the evolution of period-3 orbits (third iterate map of period-3 orbit).

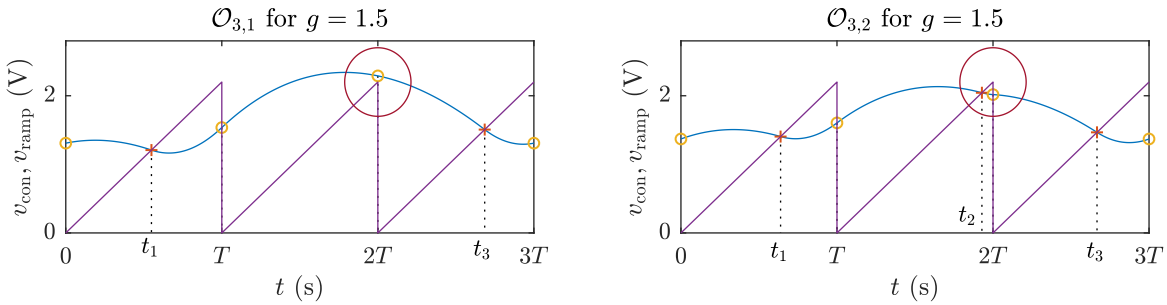

Fig. 12. Two newborn period-3 trajectories after border collision at the point A (Fig. 11) at $g = 1.5$.

In contradiction to $\mathcal{O}_{3,1}$, the unstable orbit $\mathcal{O}_{3,2}$ exists up to $g = 2.172$, where another border collision occurs (C in Fig. 11), and $\mathcal{O}_{3,3}$ is born. Like that related to the point A, this border collision

is related to equality of v_{con} and v_{ramp} at $t = 2T$; two symbolic sequences are: $(12-12-12)$ for $\mathcal{O}_{3,2}$, and $(12-1-12)$ for $\mathcal{O}_{3,3}$ (Fig. 13).

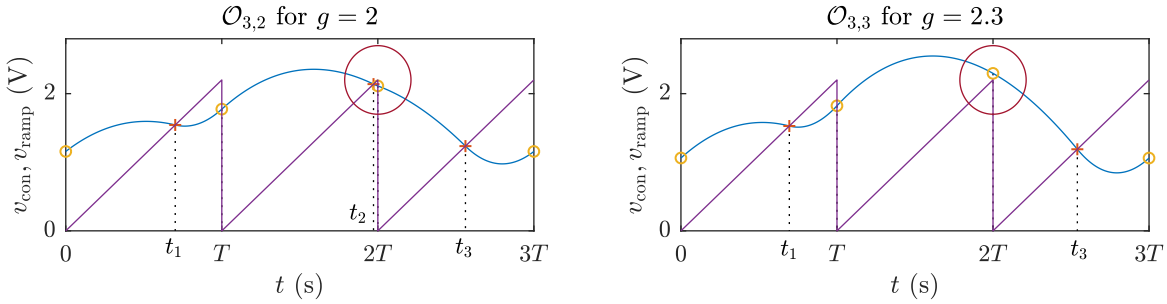

Fig. 13. Period-3 trajectories: before border collision at the point B (Fig. 11) for $g = 2$, and after border collision for $g = 2.3$.

At $g = 3.489$ (D in Fig. 11), the stable $\mathcal{O}_{3,4}$ and the unstable $\mathcal{O}_{3,5}$ orbits are born through saddle-node bifurcation that can be observed when one of the eigenvalues crosses unit circle at $+1$. Both of them are characterized by the same symbolic sequence $(121-1-12)$ as can be observed in Fig. 14. The orbit $\mathcal{O}_{3,4}$ becomes unstable at $g = 3.683$ (E in Fig. 11).

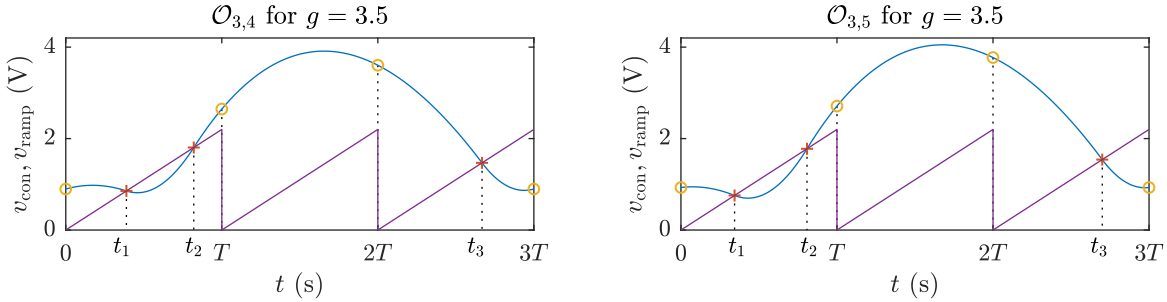

Fig. 14. Two newborn period-3 trajectories after the saddle-node bifurcation at a point D (Fig. 11) for $g = 3.5$.

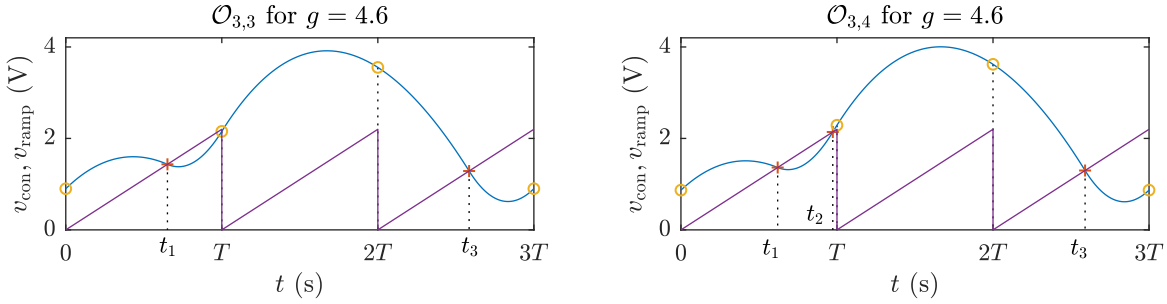

Fig. 15. Period-3 trajectories before border collision at the point F (Fig. 11) for $g = 4.6$.

At $g = 4.888$ (F in Fig. 11), both orbits $\mathcal{O}_{3,3}$ and $\mathcal{O}_{3,4}$ collapse via border collision related to the condition $v_{\text{con}} = v_{\text{ramp}}$ at $t = T$ (Fig. 15). Once again, the periodic sequences are different: $(12-1-12)$ for $\mathcal{O}_{3,3}$ and $(121-1-12)$ for $\mathcal{O}_{3,4}$.

4.5. Analysis of the period-4 orbits $\mathcal{O}_{4,i}$

Period-4 orbits demonstrate simpler behavior than those of period-3, however, three coexisting period-4 orbits may be found for the same g value (Fig. 17). Thus, at $g = 1.955$ two orbits: stable $\mathcal{O}_{4,1}$ and unstable $\mathcal{O}_{4,2}$ are born through the saddle-node bifurcation. They both coexist with an unstable $\mathcal{O}_{4,3}$ orbit (Fig. 16). The first two orbits are characterized by the periodic sequence $(121-1-1-12)$, while $\mathcal{O}_{4,3}$–by the periodic sequence $(12-1-1-12)$.

$\mathcal{O}_{4,1}$ remains stable to $g = 2.046$, when it undergoes period-doubling bifurcation and a new period-8 orbit is born (not analyzed here); finally, it disappears within a border-collision bifurcation at $g = 2.3$.

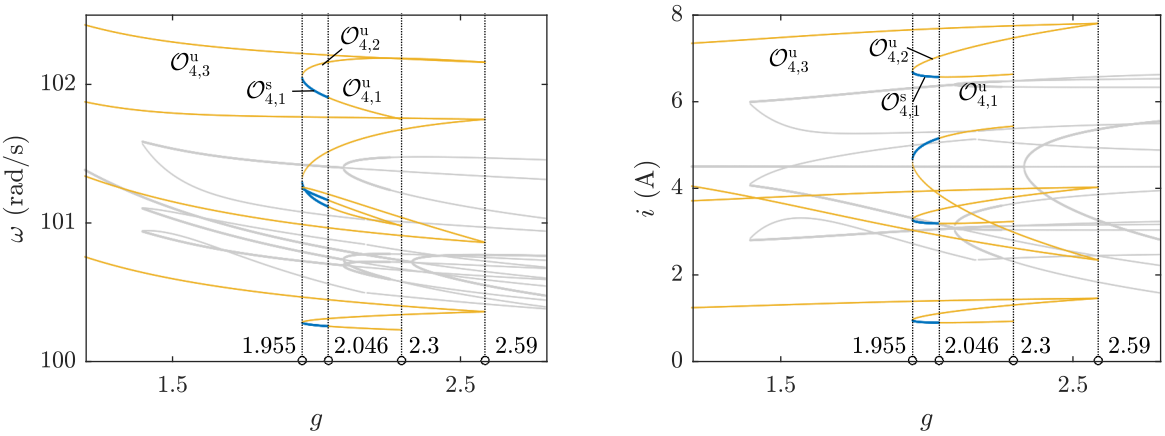

Fig. 16. Period-4 orbits of the DC drive: speed ω and current i with the change of feedback gain g; other orbits are shaded in gray.

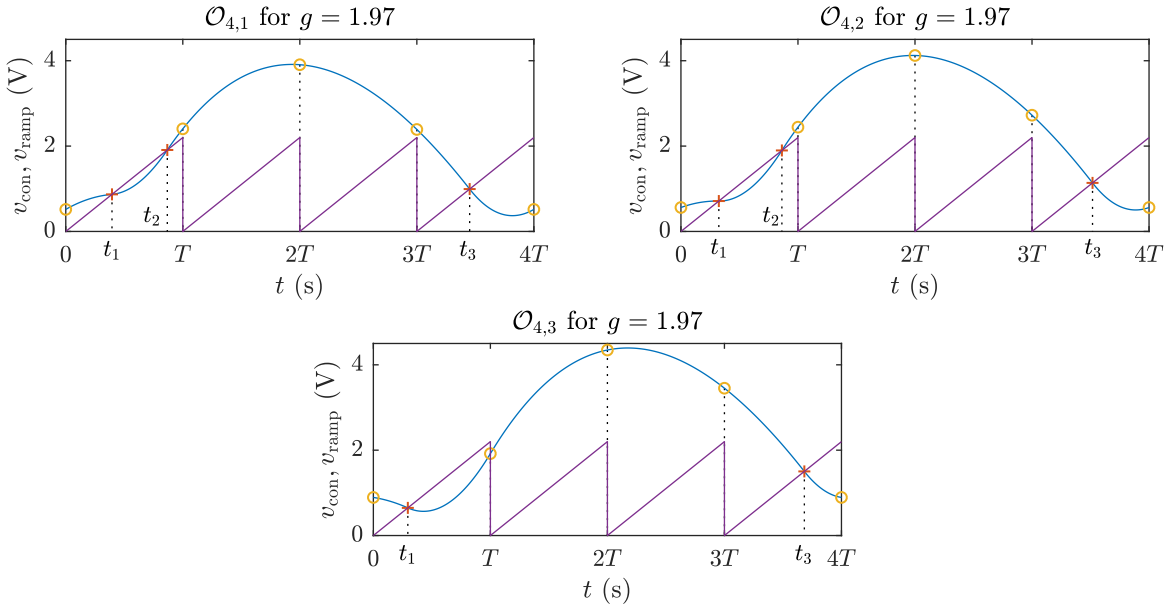

Fig. 17. Coexisting period-4 trajectories for $g = 1.97$.

The orbits $\mathcal{O}_{4,2}$ and $\mathcal{O}_{4,3}$ collapse in a border collision at $g = 2.59$ when $v_{\mathrm{con}} = v_{\mathrm{ramp}}$ at the time instant $t = T$ (Fig. 18).

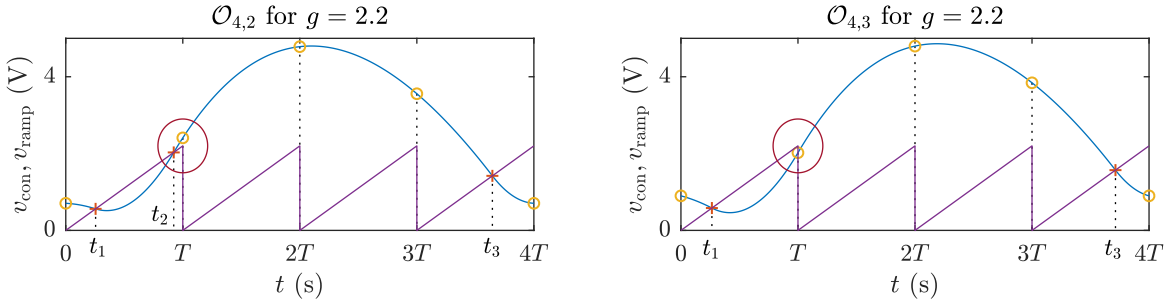

Fig. 18. Period-4 trajectories before border collision for $g = 2.2$.

4.6. Orbits of higher periods

In [6], the author provides an idea of searching all periodic solutions up to some predefined period $n\,T$ to analyze all the variety of possible nonlinear phenomena. Note, that in the present study we limit ourselves to the period-1, 2, 3 and 4 orbits. Some of the orbits of higher periods are associated with period-doubling bifurcations of a period-n orbits, when those new of period-$2\,n$ are born. For example, period-2 orbit $\mathcal{O}_{2,1}$ loses stability at $g = 2.923$, and period-4 orbit is born. Likewise, period-6 orbit is born at $g = 2.1$, while the period-3 orbit $\mathcal{O}_{3,1}$, and at $g = 2.26$, it becomes unstable causing the birth of period-12 orbit. It remains stable to $g = 2.26$, and collapses at $g = 3.21$ at border collision (Fig. 19)). Another period-6 orbit is born at $g = 3.683$, etc. However, it is preferable to accompany the analysis of periodic orbits with bifurcation diagrams obtained by the brute-force technique (by straightforward simulations omitting transients), as it was the case in [8,9]. That is the direction of our future studies.

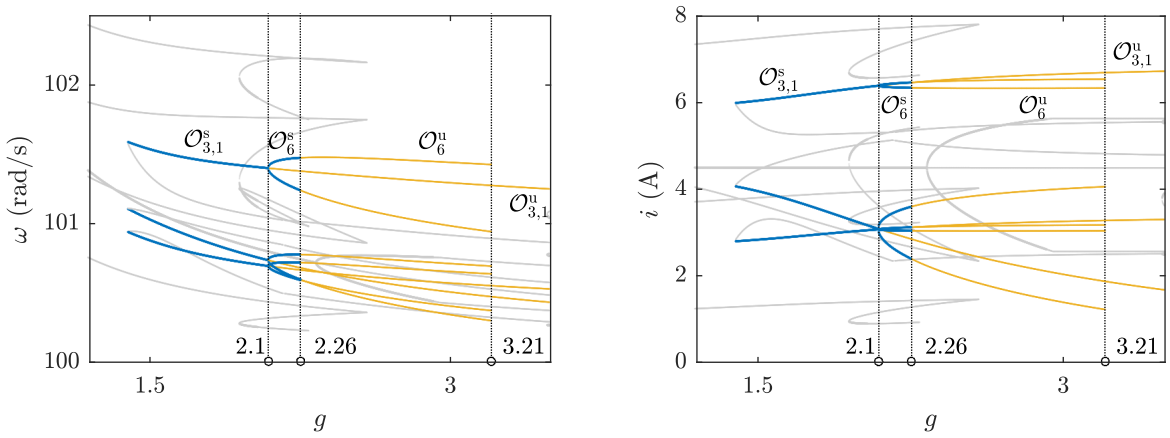

Fig. 19. Period-6 orbit along with period-3 $\mathcal{O}_{3,1}$ of the DC drive: speed ω and current i with the change of feedback gain g; other orbits are shaded in gray.

4.7. Notes on the utilization of algorithms for the continuation of periodic orbits

Above in subsection 3.2, two algorithms for the stability evaluation of periodic orbits were outlined; we name them here "manual" and "automatic." In our study, we have utilized both algorithms for the continuation of periodic orbits. However, while working with both of them, we assume, that the "automatic" algorithm is more universal; it is suitable for the detection of periodic orbits independent on their symbolic representation, because saltation matrices are computed depending on the type of the switching event without any *a priori* knowledge of the events order. However, in the presence of other coexisting periodic orbits, it may converge to another orbit, sometimes of another order.

Thus, for example, for a period-1 orbit the following condition is fulfilled: $\mathbf{x}(0) = \mathbf{x}(T)$, while for a period-$n$ orbit we have a condition $\mathbf{x}(0) = \mathbf{x}(nT)$. If the algorithm detects a period-1 orbit, it is treated as a period-n orbit, as well as the least condition is also fulfilled for a period-1 orbit.

On another hand, "manual" algorithm requires preliminary analytical work for detecting the number of crossings and their direction; however, that makes it more robust: periodic orbits of other periodicity or even other symbolic within the same periodicity remain undetected. From the practical point of view, the "manual" one may require lower values of tolerance in the Matlab ODE solver settings, that results in a faster computation.

In our studies, we have utilized "automatic" algorithm for the cases where border collision leads to the change of symbolic sequence within the orbit in order to simply detect the new orbit. The "manual" one has been used for the final computation of the exact periodic orbit, when speed and accuracy are required.

5. Discussions and conclusion

While an electric drive system should operate in a stable period-1 mode, it may demonstrate various nonlinear phenomena. In particular, for a simple chopper-fed DC drive system, the generic period-doubling scenario of losing stability is widely described since [2]. It is also known, that for the same parameter values, stable period-1, 3 and 4 orbits coexist [4]. The stability boundaries of those modes were previously studied in the literature [4].

We extend those results by analyzing unstable periodic orbits in addition to those stable, as independent on stability, they play an important role in the general structure of the state space. The continuation of periodic orbits has been performed with the use of the semi-analytical method based on Filippov theory [13].

When a stable periodic orbit is subjected to a bifurcation, that can be observed straightforward in numerical simulations. At the same time, the unstable ones are likewise subjected to bifurcations; those require special instruments to be detected. Our studies demonstrate that unstable period-2 and 3 orbits undergo persistence border collision bifurcations, when a state associated with switching instant reaches the upper value of the border (that means, control signal is equal to the ramp one exactly at $t = nT$, where $n = 1, 2, 3, \ldots$). Thus, a periodic orbit disappears and gives rise to the new periodic orbit associated with the new symbolic sequence.

Another generic scenario is demonstrated for period-3 and 4 orbits, when a border collision gives rise to the birth (or disappearance) of a couple of periodic orbits of the same periodicity but different topology. Once again, at the bifurcation point, $v_{\mathrm{con}} = v_{\mathrm{ramp}}$ exactly for $t = nT$, while for two different trajectories, control signal moves in opposite directions.

However, in our study, the effect of those bifurcations on the unstable orbits on the structure of the state space remains undiscovered.

Appendix

Table 1. Parameters of the DC drive system [2].

Parameter	**Notation**	**Value**
Ramp voltage:		
Lower level	v_{l}	0 V
Upper level	v_{u}	2.2 V
Period	T	4 ms
DC motor and load:		
Armature resistance	R	3.5 Ω
Armature inductance	L	36 mH
Back-EMF constant	K_E	0.1356 V·s
Torque constant	K_T	0.1324 N·m/A
Viscous damping	B	0.000564 N·m·s
Load inertia	J	0.000971 N·m·s^2
Load torque	T_{L}	0.39 N·m
Control system:		
Input voltage	V_{in}	100 V
Feedback gain	g	2
Reference speed	ω_{ref}	100 s^{-1}

[1] Chau K. T., Zheng W. Chaos in Electric Drive Systems: Analysis, Control and Application. Wiley-IEEE Press (2011).

[2] Chau K. T., Chen J. H., Chan C. C., Pong J. K., Chan D. T. Chaotic behavior in a simple DC drive. Proceedings of Second International Conference on Power Electronics and Drive Systems. **1**, 473–479 (1997).

[3] Okafor N., Zahawi B., Giaouris D., Banerjee S. Chaos, coexisting attractors, and fractal basin boundaries in DC drives with full-bridge converter. Proceedings of 2010 IEEE International Symposium on Circuits and Systems. 129–132 (2010).

[4] Okafor N. Analysis and Control of Nonlinear Phenomena in Electrical Drives. Ph.D. dissertation, Newcastle University, Newcastle, UK (2012).

[5] Zhang Y., Luo G. Detecting unstable periodic orbits and unstable quasiperiodic orbits in vibro-impact systems. International Journal of Non-Linear Mechanics. **96**, 12–21 (2017).

[6] Zakrzhevsky M. New concepts of nonlinear dynamics: Complete bifurcation groups, protuberances, unstable periodic infinitiums and rare attractors. J. Vibroeng. **10** (4), 421–441 (2008).

[7] Yevstignejev V., Klokov A., Smirnova R., Schukin I. Rare attractors in typical nonlinear discrete dynamical models. 2012 IEEE 4th International Conference on Nonlinear Science and Complexity (NSC). 229–234 (2012).

[8] Pikulin D. Rare phenomena and chaos in switching power converters. In: Awrejcewicz J. (eds) Applied Non-Linear Dynamical Systems. Springer Proceedings in Mathematics & Statistics. **93**, 203–211 (2014).

[9] Pikulins D., Tjukovs S., Eidaks J. Effects of control non-idealities on the nonlinear dynamics of switching DC-DC converters. In: Stavrinides S., Ozer M. (eds) Chaos and Complex Systems. Springer Proceedings in Complexity. 117–131 (2020).

[10] Filippov A. Differential Equations with Discontinuous Righthand Sides. Springer (1988).

[11] Giaouris D., Maity S., Banerjee S., Pickert V., Zahawi B. Application of Filippov method for the analysis of subharmonic instability in DC-DC converters. International Journal of Circuit Theory and Applications. **37** (8), 899–919 (2009).

[12] Baushev V., Zhusubaliyev Zh., Kolokolov Yu., Terekhin I. Local stability of periodic solutions in sampled-data control systems. Automation and Remote Control. **53** (6), 865–871 (1992).

[13] Mandal K., Chakraborty C., Abusorrah A., Al-Hindawi M. M., Al-Turki Y., Banerjee S. An automated algorithm for stability analysis of hybrid dynamical systems. Eur. Phys. J. Spec. Top. **222** (3–4), 757–768 (2013).

[14] Mandal K., Banerjee S., Chakraborty C. A new algorithm for small-signal analysis of DC-DC converters. IEEE Transactions on Industrial Informatics. **10** (1), 628–636 (2014).

[15] Hayes B., Condon M., Giaouris D. Application of the Filippov Method to PV-fed DC-DC converters modeled as hybrid-DAEs. Engineering Reports. **2** (9), e12237 (2020).

[16] Muppala K. K., Kavitha A, Duraisamy J. C. N. Analysis of intermittent instabilities in switching power converters using Filippov's method. COMPEL – The international journal for computation and mathematics in electrical and electronic engineering. **37** (6), 2025–2049 (2018).

[17] Mandal K., Abusorrah A., Al-Hindawi M. M., Al-Turki Y., El Aroudi A., Giaouris D., Banerjee S. Control-oriented design guidelines to extend the stability margin of switching converters. 2017 IEEE International Symposium on Circuits and Systems (ISCAS). 1–4 (2017).

[18] Tahir F. R., Abdul-Hassan K. M., Abdullah M. A., Pham V.-T., Hoang T. M., Wang X. Analysis and stabilization of chaos in permanent magnet DC motor driver. International Journal of Bifurcation and Chaos. **27** (11), 1750173 (2017).

[19] Ma Y., Kawakami H., Tse C. K. Bifurcation analysis of switched dynamical systems with periodically moving borders. IEEE Transactions on Circuits and Systems I: Regular Papers. **51** (6), 1184–1193 (2004).

Розрахунок стійких та нестійких періодичних орбіт у електроприводі постійного струму з ШІМ-керуванням

Кузнєцов О. О.

Національна академія сухопутних військ імені гетьмана Петра Сагайдачного, вул. Героїв Майдану, 32, 79026, Львів, Україна

Як відомо, в електроприводах проявляються різноманітні нелінійні явища. Зокрема, у приводі постійного струму з ШІМ-керуванням спостерігається перехід до хаотичної поведінки через каскад подвоєння періоду. До того ж, у такій системі проявляється співіснування декількох стійких періодичних режимів у межах стійкості основної орбіти періоду 1. Досліджено еволюцію декількох періодичних орбіт з використанням чисельно-аналітичного методу аналізу стійкості періодичних орбіт, який базується на теорії О. Філіппова. Зокрема, проаналізовано стійкі та нестійкі орбіти періодів 1, 2, 3 і 4, оскільки незалежно від стійкості, вони важливі для організації простору станів. Зокрема, у роботі показано, що нестійкі періодичні орбіти піддаються біфуркаціям граничного зіткнення відповідно до декількох загальних сценаріїв, пов'язаних із взаємодією різних орбіт того ж періоду. Ці сценарії включають біфуркації граничного зіткнення зі зміною топології орбіти, при якому періодична орбіта змінюється іншою періодичною орбітою того ж періоду; народження і зникнення пари орбіт того ж періоду, які характеризуються різною топологією.

Ключові слова: *електропривод постійного струму, стійкість, періодичні орбіти, біфуркації.*